

Direct observation of corner states in second-order topological photonic crystal slabs

Xiao-Dong Chen[†], Wei-Min Deng[†], Fu-Long Shi[†], Fu-Li Zhao, Min Chen, and Jian-Wen Dong^{*}

School of Physics & State Key Laboratory of Optoelectronic Materials and Technologies, Sun Yat-sen

University, Guangzhou 510275, China.

[†]These authors contributed equally to this work

^{*}Corresponding author: dongjwen@mail.sysu.edu.cn

Recently, higher-order topological phases that do not obey the usual bulk-edge correspondence principle have been introduced in electronic insulators and brought into classical systems, featuring with in-gap corner/hinge states¹⁻¹⁸. So far, second-order topological insulators have been realized in mechanical metamaterials⁹, microwave circuit¹⁰, topoelectrical circuit¹¹ and acoustic metamaterials^{14, 15}. Here, using near-field scanning measurements, we show the direct observation of corner states in second-order topological photonic crystal (PC) slabs consisting of periodic dielectric rods on a perfect electric conductor (PEC). Based on the generalized two-dimensional (2D) Su-Schrieffer-Heeger (SSH) model, we show that the emergence of corner states roots in the nonzero edge dipolar polarization instead of the nonzero bulk quadrupole polarization. We demonstrate the topological transition of 2D Zak phases of PC slabs by tuning intra-cell distances between two neighboring rods. We also directly observe in-gap 1D edge states and 0D corner states in the microwave regime. Our work presents that the PC slab is a powerful platform to directly observe topological states, and paves the way to study higher-order photonic topological insulators.

Topological insulators (TIs) host robust edge states predicted by the bulk-edge correspondence principle: A d -dimensional (d D) TI with d D insulating bulk states supports $(d-1)$ D conducting edge states¹⁹⁻²¹. This bulk-edge correspondence principle explains some topological properties, such as the soliton formation in polyacetylene based on the 1D SSH model²² and protected gapless edge states in 2D TIs^{23, 24}. Recently, the concept of higher-order TIs that do not obey the usual form of the bulk-edge correspondence principle have been introduced¹⁻⁵. For example, a second-order 2D TI has gapped 1D edge states but gapless 0D corner states. After the proposal in electronic insulators, higher-order topological phases have been realized in classical systems without the limitation imposed by the Fermi level. So far, 0D corner states have been observed in second-order insulators with the quantized bulk quadrupole polarization⁹⁻¹¹ or with the quantized edge dipolar polarization^{6, 14, 15}. However, the latter kind of corner states have not been experimentally observed in photonic systems.

Photonic crystals are periodic optical structures in which many fancy photonic phenomena such as negative refraction²⁵, cloaking effect²⁶, and broadband angular selectivity²⁷ were observed. With tunable geometric structures and controllable band dispersions, PCs provide a good platform to emulate the topological behaviors. For example, researchers have successfully observed the photonic analog of quantum Hall, spin Hall, and valley Hall effect in PCs²⁸⁻³⁷. However, most reported 2D topological PCs require a metallic cover in experiment to prevent the radiation of electromagnetic wave into free space. This metallic cover not only complicates the experimental setup, but also hampers the direct mapping of electromagnetic fields. In view of demands, a compact platform without the metallic cover is needed to realize the direct observation of topological states.

Here, we report the direct observation of corner states in second-order topological PC slabs consisting of periodic dielectric rods on a PEC. Our designed PC slab is free of the metallic cover,

enabling the direct observation of topological states. Moreover, this structure can not only shorten the height-diameter ratio of rods by half but also possess a full band gap, as compared with free-standing PC slabs. Based on the generalized 2D SSH model, we show that the emergence of corner states roots in the nonzero edge dipolar polarization. We demonstrate the topological transition of 2D Zak phases by expanding or shrinking four dielectric rods in the unit cell. By using near-field scanning measurements, in-gap 1D edge states and 0D corner states are directly visualized.

We first consider the free-standing square-lattice PC slab whose unit cell consists of four close-packed dielectric rods with the relative permittivity of $\varepsilon = 9.5$ in the air (Fig. 1a). The in-plane lattice constant is $a = 25$ mm, and the diameter of rods is $d = 5$ mm (inset of Fig. 1a). The height of rods is given by h , which can be tuned to change the band dispersion of PC slab. Figure 1b shows bulk band structures of the PC slab with $h = 25$ mm. Bands of TM-like and TE-like modes are marked in blue and red curves, respectively. As rod-typed PC slabs are likely to support band gaps of TM-like modes³⁸, there is a band gap between the first and second TM-like bulk bands. However, due to the small ratio between height and diameter, i.e., $h/d = 5$, the bandwidth of the TM-like band gap is 2.7%, which is too small to have a good confinement of edge states. To have a larger band gap, one can double the height of rods to be $h = 50$ mm (Fig. 1c). Figure 1d shows its bulk band structures in which a TM-like band gap ranging from 4.55 to 5.34 GHz is found. The gap width is enlarged to be 16.0% as h/d is doubled to 10. However, the large height-diameter ratio increases the difficulty of sample fabrication. In addition, there is no full band gap if one consider both TM-like and TE-like modes. These two disadvantages can be overcome by considering PC slab with periodic rods on a PEC (Fig. 1e). First, the effective height of rods will be double with the introduced PEC boundary. To see this, we consider periodic rods with $h = 25$ mm on a PEC. Figure 1f shows its bulk band structures which are exactly

the same as TM-like band dispersions of the free-standing PC slab in Fig. 1d. It confirms that the effective height of rods is double because $h = 25$ mm in Fig. 1f while $h = 50$ mm in Fig. 1d. Second, the PEC boundary requires that electric fields are perpendicular to the boundary, i.e., $E_x = E_y = 0$. Hence, TE-like modes are automatically filtered out and TM-like modes are kept (inset of Fig. 1f). As a result, a full band gap is found (shaded in blue). To prove the theoretical proposal, we construct the experimental sample in which periodic ceramic rods are put on a metallic plate (Fig. 1g). This metallic plate behaves as a PEC in the microwave regime. With the near-field scanning setup (see description in Methods), we measure E_z fields at $z = 26$ mm (e.g., see one example in Fig. 1h). E_z fields are found within the whole PC slab, proving that bulk states are excited. By performing the Fourier transform on the scanned E_z fields, we obtain the measured bulk band structures which are in good agreement with the calculated band structures (Fig. 1i).

The above discussed PC slab is the photonic realization of the 2D SSH model in which the intra-cell distances between two neighboring rods are given by d_x and d_y (Fig. 2a). By considering the first bulk band, the topology of PC slab is given by the 2D Zak phase $\mathbf{Z} = (Z_x, Z_y)$:

$$Z_j = \int dk_x dk_y \text{Tr}[\hat{A}_j(k_x, k_y)], \quad (1)$$

where $j = x$ or y , $\hat{A}_j(k_x, k_y) = i \langle u(\mathbf{k}) | \partial_{k_j} | u(\mathbf{k}) \rangle$ with $|u(\mathbf{k})\rangle$ is the periodic Bloch function. Note that, the 2D Zak phase is related to the 2D bulk polarization via $Z_j = 2\pi P_j^{18, 39}$. For PC slabs with the mirror symmetry along the j direction, Z_j is quantized to 0 and π if the origin is at the mirror plane⁴⁰. It has been proven in Ref. 40 that the Zak phase of a band is related to the symmetry of Bloch modes at the zone center and zone boundary. As the first bulk state at the Γ point is mirror symmetric, Z_x is 0 (π) when the bulk state at the X point is mirror symmetric (mirror anti-symmetric). The case of Z_y is similar by considering the bulk state at the Y point. Take the PC slab with $d_x = 5$ mm and $d_y = 5$ mm as an

example (left panel of Fig. 2c). As the bulk state at the X (Y) point is mirror symmetric (left insets of Fig. 2d), Z_x (Z_y) is 0 (0). Then this PC slab (named as PCS1 for short) is characterized by $\mathbf{Z} = (0, 0)$. We can tune d_x or d_y to achieve topological phase transitions. For example, Fig. 2d plots the frequency spectra of two lowest bulk states at the X and Y points by increasing d_y from 5 to 20 mm while keeping $d_x = 5$ mm. The mirror symmetric and anti-symmetric states are labelled in red and blue, respectively. The lowest bulk state at the X point keeps mirror-symmetric as there is no mode exchange. On the contrary, two bulk states at the Y point move closer, touch, and separate with the increasing of d_y . After the mode exchange at $d_y = 12.5$ mm, PC slab is characterized by $Z_y = \pi$ as the lowest bulk state at the Y point becomes mirror anti-symmetric. One representative PC slab with $d_x = 5$ mm and $d_y = 20$ mm is shown in the middle panel of Fig. 2c and named as PCS2. Similarly, PC slabs with $Z_x = \pi$ can be obtained when $d_x > 12.5$ mm. Because both Z_x and Z_y are either 0 or π , PC slabs are classified into four different topological phases (Fig. 2b). Particularly, we can obtain PC slabs with nonzero Zak phase along both two directions, e.g., PC slab with $d_x = 20$ mm and $d_y = 20$ mm (right panel of Fig. 2c and named as PCS3). To see the phase transition from PCS1 to PCS3, we consider PC slabs by increasing d_y and keeping $d_x = d_y$. Figure 2e plots the frequency spectra of two lowest bulk states at the X and Y points. After the mode exchange at both two k -points, PC slabs are characterized by $\mathbf{Z} = (\pi, \pi)$ as the lowest bulk states become mirror anti-symmetric (right insets of Fig. 2e).

The topological distinction between PC slabs with different Z_j guarantees the existence of edge states. As Z_y is 0 for PCS1 while it is π for PCS2 (or PCS3), there are edge states along the x direction for the boundary between PCS1 and PCS2 (or PCS3). To verify this prediction, we first construct the boundary between PCS1 and PCS2 (Fig. 3a). We put the source antenna at the left and scan E_z fields (see Supplementary Fig. S1). By performing the Fourier transform of the measured E_z fields, the

dispersion of edge states is shown by the bright color in Fig. 3b. The measured edge band dispersion agrees well with the simulated dispersion marked by the green line. Gapped edge states are confirmed as the dispersion does not cover the whole bulk band gap. In addition, with the measured E_z fields at the frequencies of 4.39 GHz (i.e., at $k_x = 0$) and 5.18 GHz (i.e., at $k_x = \pi/a$), we can retrieve the eigen-fields of edge states at the zone center and boundary (Fig. 3c). Both edge states at the zone center and boundary are mirror symmetric, indicating the zero edge dipolar polarization. To have a nonzero edge dipolar polarization, we consider the boundary between PCS1 and PCS3 (Fig. 3d). We also scan E_z fields (see Supplementary Fig. S2) and obtain the measured edge dispersion which is in good agreement with the calculated dispersion (Fig. 3e). Gapped edge states are found but their dispersion curve is different to that in Fig. 3b, indicating that they have different features. To see this, we retrieve the eigen-fields of edge states at $k_x = 0$ at the frequency of 4.41 GHz and at $k_x = \pi/a$ at the frequency of 4.84 GHz (Fig. 3f). Edge state at the zone center is mirror symmetric while that at the zone boundary is mirror anti-symmetric. It confirms the nonzero edge dipolar polarization. Note that the distinction between edge dipolar polarizations of two boundaries is inherent from the topological distinction between 2D Zak phases of PCS2 and PCS3.

The nonzero edge dipolar polarization between PCS1 and PCS3 indicates the existence of corner states. To verify this prediction, we construct the experimental sample for observing corner states (Fig. 4a). It consists of the PCS3 at the center while the PCS1 at the background. In experiment, we put a source antenna near the top-right corner and measure E_z fields at $z = 26$ mm. For example, Figure 4b shows the measured E_z fields at $f = 4.01$ GHz (see more E_z fields in Supplementary Fig. S4). To identify bulk, edge, and corner states, we apply three binary filters (lower panel of Fig. 4b) to separate responses of different eigen-states. Figure 4c shows the resulting spectra in which high values indicate the

existence of eigen-states and zero (or low) values mean the presence of band gaps. Within the bulk and edge gaps, a resonance of the corner spectrum is found near 5.2 GHz. It corresponds to the corner state whose existence has been predicted according to the nonzero edge dipolar polarization (Fig. 4d). The zoom-in E_z fields clearly demonstrate that fields of the corner state are concentrated around the top-right single rod (left panel of Fig. 4e). The field concentration can be also achieved by considering the frequency within the bulk, edge, and corner gaps, e.g., localized state at $f = 4.98$ GHz (right panel of Fig. 4e). But these two field concentrations are different because corner states are immune to the source position while localized states are dependent on the source position. Lastly, we carry out a comparative study of the sample without corner states (Fig. 4f). Within the bulk and edge gaps, there is no resonance of corner spectra. It proves the absence of corner states due to the zero edge dipolar polarization between PCS1 and PCS2. More detailed discussion including the presence (absence) of edge states at the top (right) boundary is given in Supplementary Fig. S5. Note that we only discuss the top-right corner as the other three corners have the same corner states protected by the C_4 -rotation symmetry.

In conclusion, we design and demonstrate a new type of PC slabs by putting periodic dielectric rods on a PEC. Based on the 2D SSH model, we illustrate the topological phase map of 2D Zak phases and the topological phase transition. Inherent from the nonzero Zak phase of bulk states, we directly observe corner states induced by the nonzero edge dipolar polarization. This is the smoking-gun feature of second-order topological PC slabs in which 0D corner states are predicted by the nontrivial Zak phase of 2D bulk states. Our results demonstrate that second-order photonic TIs can guide the light flow and trap the light. The localized corner state may have the potential application in enhancing light-matter interaction, which is desirable for many nanophotonic devices.

Methods

Experimental measurement. The dielectric rods are made of ceramic whose relative permittivity is $\epsilon = 9.5$. The height of rods is $h = 25$ mm and the diameter is $d = 5$ mm. In the experiment, the in-plane lattice constant of PC slabs was kept as $a = 25$ mm, and there are four rods in one unit cell. Periodic rods were put on a metallic plate (made of aluminum) which behaves as the PEC in the microwave frequency. Samples for measuring edge states in Fig. 3 and corner states in Fig. 4 have the in-plane size of $20a \times 20a$. To precisely locate 1600 rods, a paper with the printed in-plane pattern of circles was put on the metallic plate, and all rods are glued to the paper. Note that the thickness of paper is about 0.2 mm, and it changes little the band structures and has no influence on the topology of PC slabs.

The schematic of the near-field scanning setup is shown in Fig. 1g. A source antenna was inserted through the drilled hole in the metallic substrate to excite eigen-states of PC slabs. The signal was measured by a probe antenna along the z direction, and the measured E_z fields were collected by the vector network analyzer (Agilent E5071C). To image E_z fields in free space (i.e., in the xy and xz planes), the probe antenna was mounted on a three-dimensional motorized translation stage (LINBOU NFS03). To avoid the collision between the probe antenna and rods, we measured E_z fields above the plane which is slightly higher than the top of rods, i.e., $z \geq 26$ mm. The scanning resolution was 2 mm along all directions.

Data analysis. To retrieve E_z fields of edge states at $k_x = 0$ and $k_x = \pi/a$ in Figs. 3c and 3f, we first transformed the measured fields $E_z(x, y)$ by the transformation of $e_z(k_x, y) = \sum_{n=0}^N E_z(n\Delta x, y)e^{-ik_x \cdot n\Delta x}$, where Δx is the scanning resolution along the x direction and N is

the step number of the transformation region. As $\Delta x = a/12.5$, we considered k_x from $-6.25 \times 2\pi/a$ to $6.25 \times 2\pi/a$. To avoid the influence of the left/right boundaries and the source antenna, we chose the transformation region from $x = 5a$ to $x = 15a$. By keeping $k_x = k_x^0 + 2m\pi/a$ ($m \in Z$) and filtering out other k_x components, E_z fields at k_x^0 were retrieved by the inverse transformation of $E_z(x, y)_{k_x^0} = \sum_m e_z(k_x^0 + 2m\pi/a, y) e^{i(k_x^0 + 2m\pi/a) \cdot x}$.

To identify bulk, edge, and corner responses in Fig. 4c, the bulk binary filter has the size of $200 \times 200 \text{ mm}^2$, the edge binary filter has the size of $2 \times 20 \times 200 \text{ mm}^2$, and the corner binary filter has the size of $20 \times 20 \text{ mm}^2$. To obtain spectra in Fig. 4f, the bulk and corner binary filters have the same sizes of those in Fig. 2b, while the top-edge and right-edge binary filters have the size of $20 \times 200 \text{ mm}^2$.

Numerical simulation. The first principle electromagnetic simulations were performed with the COMSOL Multiphysics. An eigenfrequency study was used to calculate band structures. The perfect electric conductor boundary condition was applied when the metallic substrate was considered.

Data availability

The data that support the findings of this study are available from the corresponding author upon reasonable request.

REFERENCES

1. Benalcazar, W.A., Bernevig, B.A. & Hughes, T.L. Electric multipole moments, topological multipole moment pumping, and chiral hinge states in crystalline insulators. *Physical Review B* **96**, 245115 (2017).
2. Benalcazar, W.A., Bernevig, B.A. & Hughes, T.L. Quantized electric multipole insulators. *Science* **357**, 61-66 (2017).
3. Langbehn, J., Peng, Y., Trifunovic, L., von Oppen, F. & Brouwer, P.W. Reflection-Symmetric

- Second-Order Topological Insulators and Superconductors. *Physical Review Letters* **119**, 246401 (2017).
4. Song, Z., Fang, Z. & Fang, C. (d-2)-Dimensional Edge States of Rotation Symmetry Protected Topological States. *Physical Review Letters* **119**, 246402 (2017).
 5. Schindler, F. et al. Higher-order topological insulators. *Science advances* **4**, 0346 (2018).
 6. Ezawa, M. Higher-Order Topological Insulators and Semimetals on the Breathing Kagome and Pyrochlore Lattices. *Physical Review Letters* **120**, 026801 (2018).
 7. Geier, M., Trifunovic, L., Hoskam, M. & Brouwer, P.W. Second-order topological insulators and superconductors with an order-two crystalline symmetry. *Physical Review B* **97**, 205135 (2018).
 8. Kunst, F.K., Miert, G.v. & Bergholtz, E.J. Lattice models with exactly solvable topological hinge and corner states. *Physical Review B* **97**, 241405 (2018).
 9. Serra-Garcia, M. et al. Observation of a phononic quadrupole topological insulator. *Nature* **555**, 342-345 (2018).
 10. Peterson, C.W., Benalcazar, W.A., Hughes, T.L. & Bahl, G. A quantized microwave quadrupole insulator with topologically protected corner states. *Nature* **555**, 346-350 (2018).
 11. Imhof, S. et al. Topoelectrical-circuit realization of topological corner modes. *Nature Physics* **14**, 925-929 (2018).
 12. Noh, J. et al. Topological protection of photonic mid-gap defect modes. *Nature Photonics* (2018).
 13. Li, F.-F. et al. Topological light-trapping on a dislocation. *Nature communications* **9**, 2462 (2018).
 14. Xue, H., Yang, Y., Gao, F., Chong, Y. & Zhang, B. Acoustic higher-order topological insulator on a Kagome lattice. *arXiv* **1806.09418** (2018).
 15. Ni, X., Weiner, M., Alù, A. & Khanikaev, A.B. Observation of Bulk Polarization Transitions and Higher-Order Embedded Topological Eigenstates for Sound. *arXiv* **1807.00896** (2018).
 16. Zhang, X. et al. Observation of second-order topological insulators in sonic crystals. *arXiv* **1806.10028** (2018).
 17. Zhang, X. et al. Acoustic Hierarchical Topological Insulators. *arXiv* **1811.05514** (2018).
 18. Xie, B.-Y. et al. Second-order photonic topological insulator with corner states. *Physical Review B* **98**, 205147 (2018).
 19. Qi, X.-L. & Zhang, S.-C. Topological insulators and superconductors. *Reviews of Modern Physics* **83**, 1057-1110 (2011).
 20. Xiao, D., Chang, M.-C. & Niu, Q. Berry phase effects on electronic properties. *Reviews of Modern Physics* **82**, 1959-2007 (2010).
 21. Hasan, M. & Kane, C. Colloquium: Topological insulators. *Reviews of Modern Physics* **82**, 3045-3067 (2010).
 22. Su, W.P., Schrieffer, J.R. & Heeger, A.J. Solitons in Polyacetylene. *Physical Review Letters* **42**, 1698-1701 (1979).
 23. Kane, C.L. & Mele, E.J. Z₂ Topological Order and the Quantum Spin Hall Effect. *Physical Review Letters* **95** (2005).
 24. Manoharan, H.C. Topological insulators: A romance with many dimensions. *Nature Nanotechnology* **5**, 477-479 (2010).
 25. Cubukcu, E., Aydin, K., Ozbay, E., Foteinopoulou, S. & Soukoulis, C.M. Negative refraction by photonic crystals. *Nature* **423**, 604-605 (2003).
 26. Huang, X., Lai, Y., Hang, Z.H., Zheng, H. & Chan, C.T. Dirac cones induced by accidental degeneracy in photonic crystals and zero-refractive-index materials. *Nature Materials* **10**, 582

- (2011).
27. Shen, Y. et al. Optical broadband angular selectivity. *Science* **343**, 1499-1501 (2014).
 28. Wang, Z., Chong, Y., Joannopoulos, J.D. & Soljačić, M. Observation of unidirectional backscattering-immune topological electromagnetic states. *Nature* **461**, 772-775 (2009).
 29. Poo, Y., Wu, R.-x., Lin, Z., Yang, Y. & Chan, C.T. Experimental realization of self-guiding unidirectional electromagnetic edge states. *Physical Review Letters* **106**, 093903 (2011).
 30. Khanikaev, A.B. et al. Photonic topological insulators. *Nature Materials* **12**, 233 (2012).
 31. Chen, W.-J. et al. Experimental realization of photonic topological insulator in a uniaxial metacrystal waveguide. *Nature communications* **5**, 5782 (2014).
 32. Wu, L.-H. & Hu, X. Scheme for achieving a topological photonic crystal by using dielectric material. *Physical Review Letters* **114**, 223901 (2015).
 33. Yang, Y. et al. Visualization of a Unidirectional Electromagnetic Waveguide Using Topological Photonic Crystals Made of Dielectric Materials. *Physical Review Letters* **120**, 217401 (2018).
 34. Barik, S. et al. A topological quantum optics interface. *Science* **359**, 666-668 (2018).
 35. Ma, T. & Shvets, G. All-si valley-Hall photonic topological insulator. *New Journal of Physics* **18**, 025012 (2016).
 36. Dong, J.-W., Chen, X.-D., Zhu, H., Wang, Y. & Zhang, X. Valley photonic crystals for control of spin and topology. *Nature Materials* **16**, 298-302 (2017).
 37. Chen, X.-D., Zhao, F.-L., Chen, M. & Dong, J.-W. Valley-contrasting physics in all-dielectric photonic crystals: Orbital angular momentum and topological propagation. *Physical Review B* **96**, 020202(R) (2017).
 38. Joannopoulos, J.D., Johnson, S.G., Winn, J.N. & Meade, R.D. Photonic crystals - molding the flow of light, Vol. 2nd ed. (Princeton University Press, Princeton, NJ, 2008).
 39. Liu, F. & Wakabayashi, K. Novel Topological Phase with a Zero Berry Curvature. *Physical Review Letters* **118** (2017).
 40. Xiao, M., Zhang, Z.Q. & Chan, C.T. Surface impedance and bulk band geometric phases in one-dimensional systems. *Physical Review X* **4**, 021017 (2014).

Acknowledgements

This work was supported by National Natural Science Foundation of China (Grant Nos. 11704422, 61775243, 11522437, 61471401, and 11761161002), Natural Science Foundation of Guangdong Province (Grant No. 2018B030308005), and Science and Technology Program of Guangzhou (Grant No. 201804020029).

Author contributions

X.-D.C and J.-W.D conceived the idea and designed the experiment. W.-M.D and X.-D.C completed the numerical simulations. F.-L.S carried out the microwave experiment. J.-W.D supervised the project. All authors contributed to the theoretical discussions, the experimental data analysis, and the manuscript writing.

Competing financial interests

The authors declare no competing financial interests.

Additional information

Supplementary information is available in the online version of the paper. Correspondence and requests for materials should be addressed to J.-W.D.

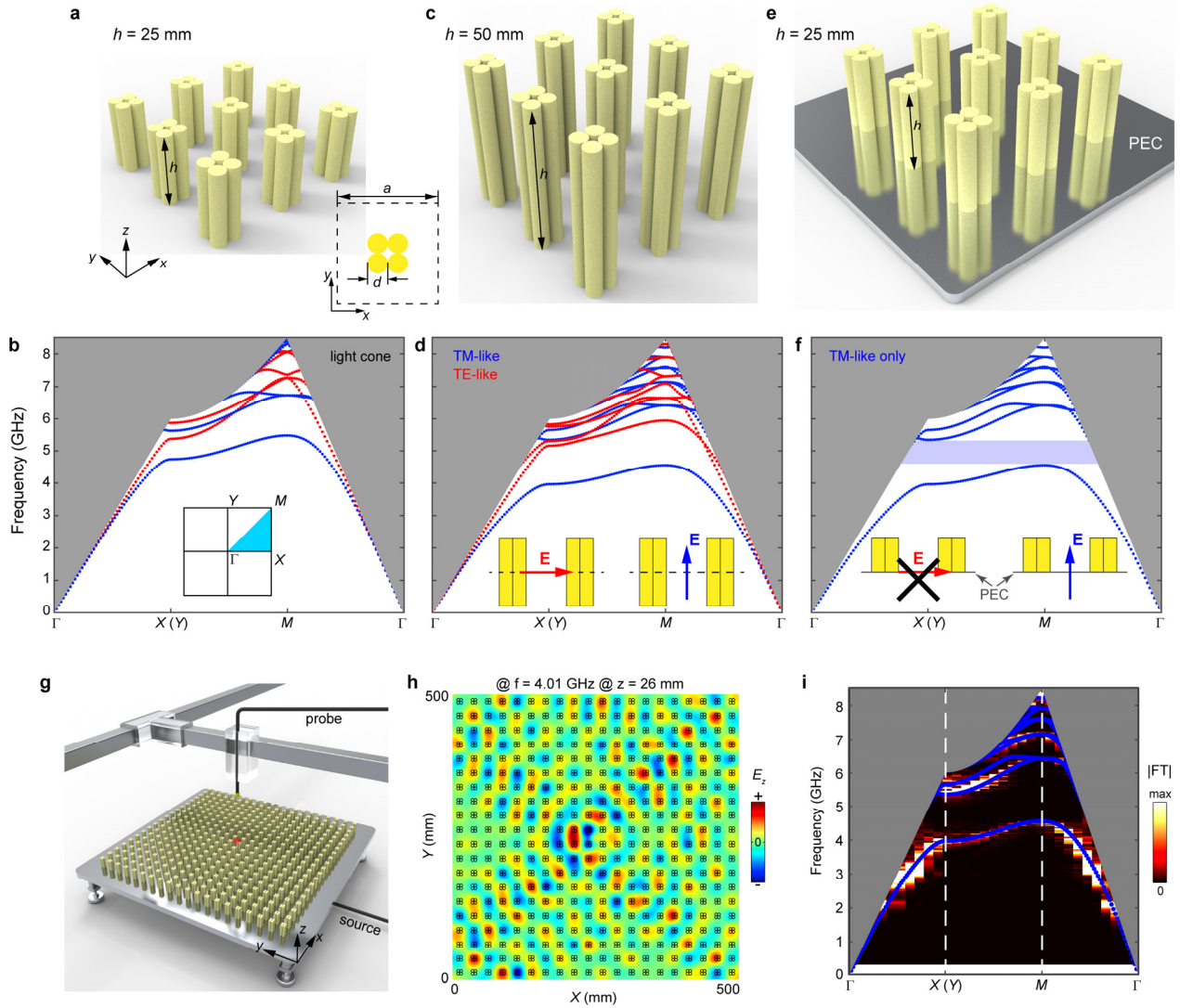


Figure 1 | Photonic crystal (PC) slabs with periodic dielectric rods standing on a perfect electric conductor (PEC). **a-d**, Schematics and bulk band structures of free-standing PC slabs with **(a, b)** $h = 25$ mm, and **(c, d)** $h = 50$ mm. All dielectric rods with $\epsilon = 9.5$ have the diameter of $d = 5$ mm, and the in-plane lattice constant is $a = 25$ mm (inset in **a**). The inset in **(b)** illustrates the Brillouin zone. The insets in **(d)** illustrate that electric fields of TE-like and TM-like modes are in-plane and out-of-plane at the central plane. Bands of TM-like and TE-like modes are marked in blue and red curves, respectively. The light cone is shaded in grey. **b**, Due to the small height-diameter ratio (i.e., h/d) of 5, the bandwidth of the first TM-like band gap is 2.7%. **d**, The bandwidth of TM-like band gap can be increased to 16.0% by doubling h/d ratio to 10 which is too large for the sample fabrication. In addition, there is no full band gap in free-standing PC slabs if one considers both TM-like and TE-like modes. **e-f**, Schematic and bulk band structure of the PC slab with periodic dielectric rods standing on a PEC. Only TM-like modes exist, as TE-like modes are filtered out by the additional PEC boundary condition (inset in **f**). Hence, a full band gap is found (shaded in blue). In addition, bulk bands in **(f)** have the same 16.0% band gap as those in **(d)**, although the height of rods in **(e)** is only half of that in **(c)**. **g**, Experimental setup for the near-field scanning measurement. Periodic ceramic rods stand on a metallic plate which behaves as a PEC at the microwave frequency. A probe antenna is mounted on a motorized translation stage to scan electric fields in free space, whilst a source antenna (marked in red) is inserted

through the drilled hole in the metallic substrate to excite bulk states. **h**, Measured E_z fields at $z = 26$ mm (at an arbitrary frequency of $f = 4.01$ GHz), which are then performed with the Fourier transform to get the dominated components in the reciprocal k -space. **i**, The measured (bright color) and calculated (blue line) bulk band structures. The good agreement between the experimental and simulated results is found.

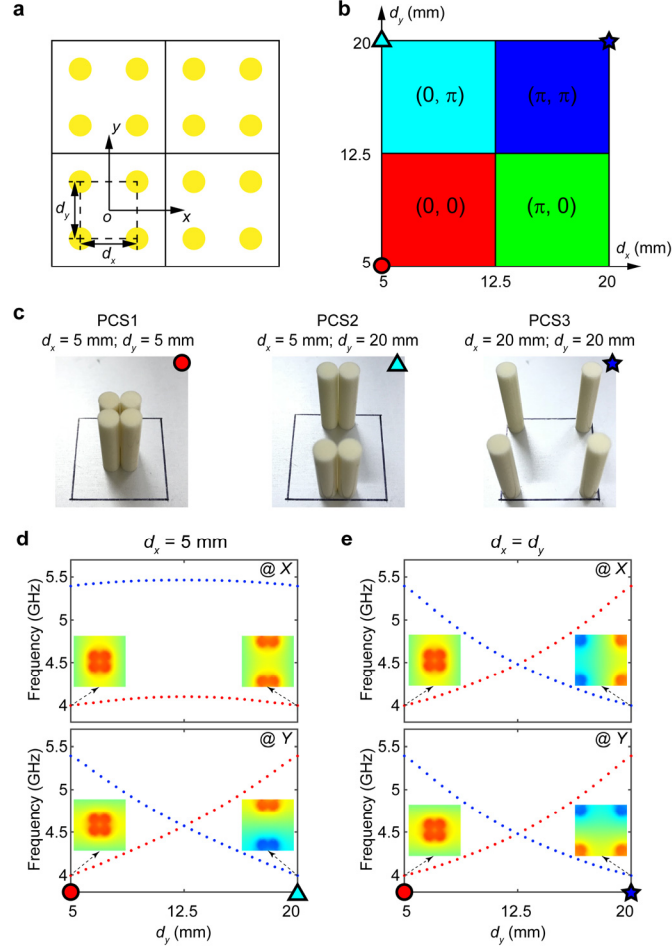


Figure 2 | Topological transition of 2D Zak phase of the PC slab. **a**, Schematic of the PC slab with four unit cells in the xy plane. The origin is defined at the center of the unit cell. The distance between two neighboring rods along the x and y directions are d_x and d_y , respectively. To keep quantized Z_x and Z_y , we preserve the mirror symmetries along the x and y directions during the changing of d_x and d_y . **b**, Classification of PC slabs based on the 2D Zak phase $\mathbf{Z} = (Z_x, Z_y)$. PC slabs with d_x and d_y ranging from 5 to 20 mm are classified into four regions. Three representative PC slabs (whose unit cells are given in **c**) are labelled by the red circle, cyan triangle and blue star, respectively. **c**, Zoom-in photos of three representative PC slabs with (left) $d_x = 5$ mm, $d_y = 5$ mm, named as PCS1, (middle) $d_x = 5$ mm, $d_y = 20$ mm, named as PCS2, and (right) $d_x = 20$ mm, $d_y = 20$ mm, named as PCS3. **d-e**, Evolution of two lowest bulk states at the X and Y points as a function of d_y whilst (**d**) keeping $d_x = 5$ mm or (**e**) keeping $d_x = d_y$. Mirror symmetric (anti-symmetric) states are marked in red (blue) dots. In (**d**), mode exchange happens at the Y point but not the X point. It results in the change of Z_y but not Z_x . While in (**e**), mode exchange happens at both the X point and the Y point. It leads to the change of both Z_x and Z_y . E_z fields of the first lowest bulk states of each PC slab are given as insets.

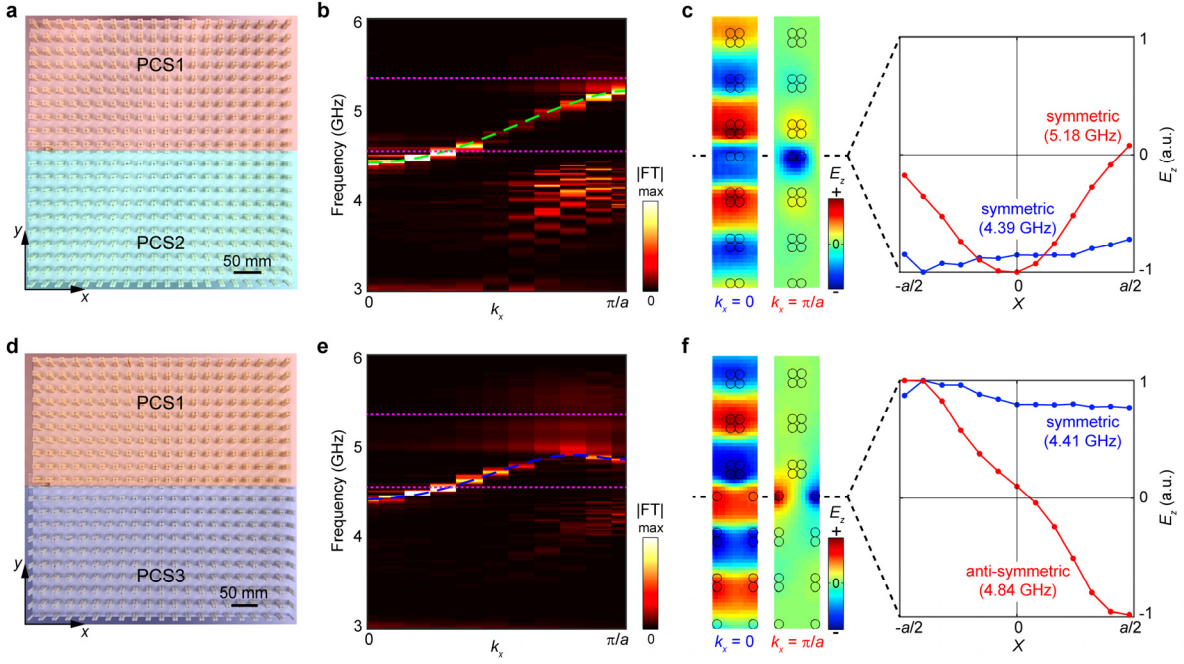


Figure 3 | Gapped edge states with zero and nonzero edge dipolar polarization. **a**, The photo (top-view) of the boundary between PCS1 and PCS2. **b**, The measured (bright color) and calculated (green line) gapped edge band dispersions. Two pink dash lines mark the lower and upper frequencies of the bulk band gap. **c**, The retrieved E_z fields at the zone center ($k_x = 0$) and zone boundary ($k_x = \pi/a$). Both E_z fields at the zone center and zone boundary are mirror symmetric with respect to the central yz plane. **d**, The photo (top view) of the boundary between PCS1 and PCS3. **e**, The measured (bright color) and calculated (blue line) gapped edge band dispersions. Two pink dash lines mark the lower and upper frequencies of the bulk band gap. **f**, The retrieved E_z fields at the zone center ($k_x = 0$) and zone boundary ($k_x = \pi/a$). Edge state at zone center is mirror symmetric, while that at zone boundary is mirror anti-symmetric.

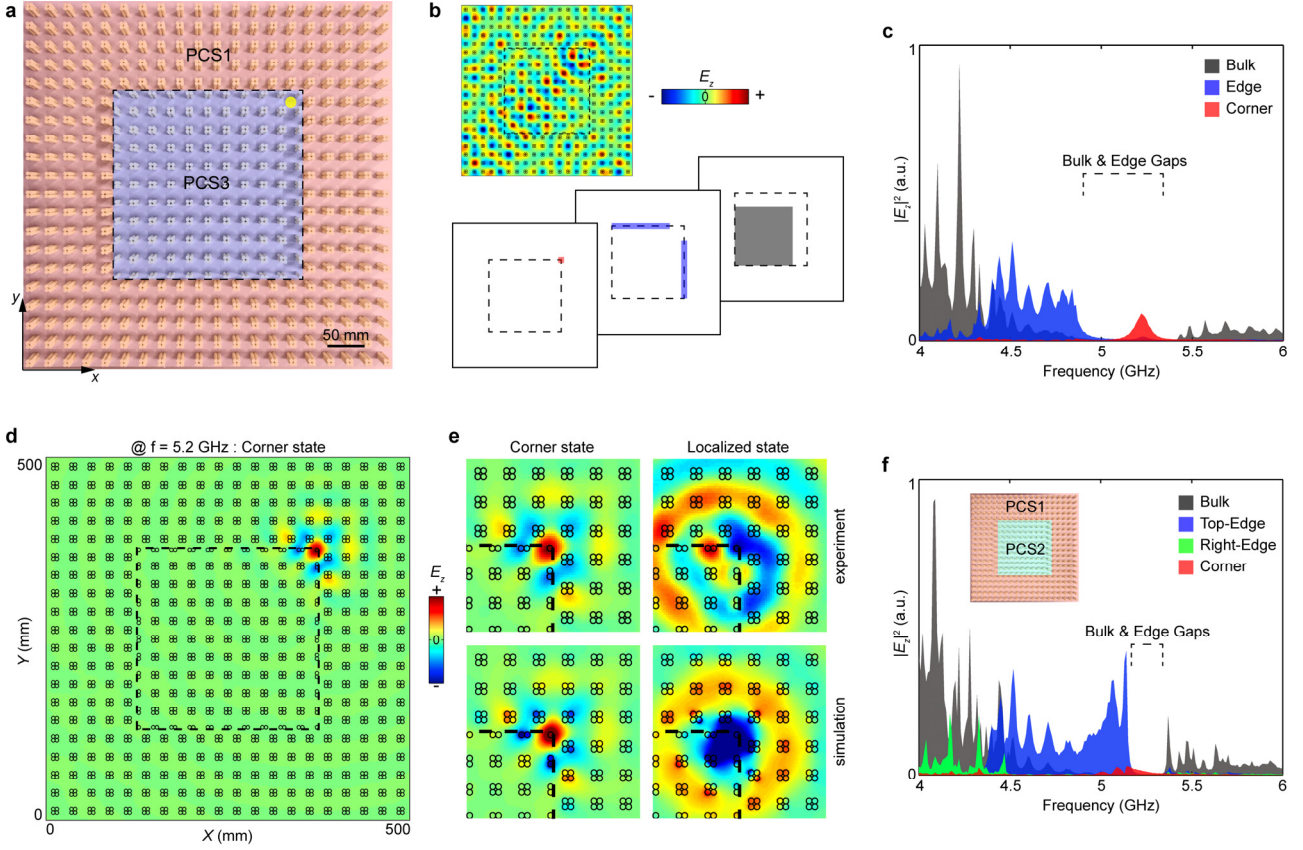


Figure 4 | Direct observation of corner states. **a**, The photo (top view) of the experimental sample for measuring topological corner states. It consists of the PCS3 at the center while the PCS1 at the background, with the black dash square indicating boundaries. The yellow dot marks the position of the source antenna. **b**, The response of the sample at an arbitrary frequency (4.01 GHz). The square of measured E_z fields, i.e., $|E_z|^2$ are multiplied by three binary filters shown below to determine the bulk (grey), edge (blue) and corner (red) responses at different frequencies. **c**, The resulting spectra of bulk, edge, and corner states, showing different resonant frequencies. **d**, Measured E_z fields of the corner state at 5.2 GHz. **e**, Experimentally measured (top) and numerically simulated (bottom) E_z fields of the corner and localized states are shown in the left and right panels, respectively. **f**, The bulk, edge, and corner spectra of the sample without corner states. The inset shows the sample constructing by PCS1 and PCS2. There is no resonance of the corner spectrum in bulk and edge gaps.